ELSEVIER

Ceramics International 25 (1999) 395–408

CERAMICS INTERNATIONAL

Review: High temperature deformation of Al_2O_3-based ceramic particle or whisker composites

Q. Tai *, A. Mocellin

LSG2M, UMR 7584, Ecole des Mines, Parc de Saurupt, F-54042 Nancy Cedex, France

Received 6 September 1997; accepted 17 November 1997

Abstract

The major theoretical models for creep and the creep rate equations of ceramic materials and their dispersed phase composites are briefly reviewed. Then the literature on high temperature deformation behaviours of Al_2O_3-based oxide ceramic particle composites (Al_2O_3-ZrO_2, Al_2O_3-$Y_3Al_5O_{12}$, Al_2O_3-Tio_2) and Al_2O_3-based non-oxide ceramic particle or whisker composites (Al_2O_3-$SiC_{(w)}$, Al_2O_3-$SiC_{(p)}$, Al_2O_3-TiC_xN_{1-x}) since the mid 1980s is reviewed. Most studies have been concerned with the Al_2O_3-ZrO_2 and Al_2O_3-SiC systems. The influences of various factors on the creep behaviours, the changes of the microstructure in the deformed specimens and the creep mechanisms of these composites are summarised and analysed.

1. Introduction

In recent years, structural ceramic materials have attracted much attention, because of their excellent mechanical properties such as high strength, hardness, anti-abrasion, chemical stability and heat resistance. There has been a recognition of the potential of structural ceramics for use both in high temperature applications in advanced heat engine and heat exchangers and in ambient temperature applications in cutting tools, and wear parts. The disadvantage of ceramics is their low fracture toughness and poor mechanical reliability which so far have limited their practical applications. Thus, methods to improve their fracture toughness and retain their high-temperature creep properties as well as enhance their mechanical reliability are a major challenge. One way to achieve these goals is through the development of composite structures. That is to the ceramic matrices are added dispersed ceramic particles, whiskers or fibres which reinforce the matrices and improve their mechanical properties.

Alumina-based ceramic composites such as Al_2O_3-Zr02, Al_2O_3-$Y_3Al_5O_{12}$, Al_2O_3-SiC, Al_2O_3-TiC, Al_2O_3-TiC_xN_{1-x} composites are widely studied, as to their ambient and high temperature mechanical properties and reliabilities. Great emphasis is placed on their high temperature creep behaviours.

The purpose of this paper is to recall briefly the major theoretical models for creep and then to review the available information on the plastic deformation behaviours of Al_2O_3-based ceramic composites. Composites reinforced by long fibres are not discussed here since their fabrication procedures markedly differ from those based on powder processing which yield materials with dispersed phases.

2. Deformation mechanisms

2.1. The rate equations for plastic deformation

The high temperature creep of single phase crystalline materials may be expressed by a relationship of the following form:

$$\dot{\varepsilon} = A\frac{DGb}{kT}\left(\frac{b}{d}\right)^p\left(\frac{\sigma}{G}\right)^n \quad (1)$$

where $\dot{\varepsilon}$ is the steady state creep rate, A is a dimensionless constant, D is the appropriate diffusion coefficient, G is the shear modulus, b is the magnitude of the Burgers vector, k is Boltzmann's constant, T is the absolute temperature, d is the grain size, σ is the applied stress,

* Corresponding author at Nanjing University of Chemical Technology, 210009, Nanjing, People's Republic of China.

0272-8842/99/$20.00
PII: S0272-8842(98)00017-0

and p and n are constants termed the inverse grain size exponent and the stress exponent, respectively. The diffusion coefficient D may be expressed as $Do \exp(-Q/RT)$, where Do is a frequency factor, Q is the apparent activation energy, and R is the gas constant.

For two phase composites, there are several equations which may express or predict their high temperature creep behaviours.

In composites, where the second phase can be considered rigid, Raj and Ashby model [1] assumes that the hard second phase particles in the grain boundary of matrix limit the grain boundary sliding and gives:

$$\dot{\varepsilon} = \mathrm{C}\frac{\sigma^{\mathrm{n}}}{\mathrm{d}^{\mathrm{p}}\mathrm{r}^{\mathrm{q}}\mathrm{V}}\exp\left(-\frac{\mathrm{Q}}{\mathrm{RT}}\right) \tag{2}$$

where V is the second phase volume content, r is second phase grain radius, q and n are phenomenological exponents and C is a constant.

Chen model [2] considers the composites as a model system of a soft matrix containing equiaxed and rigid inclusions. Based on a phenomenological constitutive equation and a second phase continuum mechanics model, his model gives:

$$\dot{\varepsilon} = \dot{\varepsilon}_{\mathrm{o}}(1-\mathrm{V})^{2+\mathrm{n}/2} \tag{3}$$

where V is the second phase volume content, $\dot{\varepsilon}_o$ is the strain rate of the reference matrix, n is the stress exponent of the matrix.

Ravichandran and Seetharaman model [3] considers that a rigid and noncreeping second phase distributes uniformly in a continuous creeping matrix, and they develop a simple continuum mechanics model to predict the steady state creep rates of composites:

$$\dot{\varepsilon} = \mathrm{A}\left[\frac{\sigma(1+\mathrm{C})^2}{\left(\frac{(1+\mathrm{C})^{1/\mathrm{n}}}{\mathrm{C}}\right)+(1+\mathrm{C})^2-1}\right]^{\mathrm{n}} \tag{4}$$

where $C = \left[\frac{1}{V}\right]^{1/3} - 1$, V is the second phase volume content, n is the stress exponent of the matrix, A is the constant of the matrix.

For a two phase composite in which each phase undergoes diffusional creep, Wakashima and Liu give a viscoelastic constitutive equation corresponding to a spring-dashpot model [4]:

$$\varepsilon = \left[\frac{\Delta E}{E_u}\left\{1-\exp\left(-\frac{t}{\tau}\right)\right\}+\frac{1}{\bar{\eta}}\right]\sigma \tag{5}$$

where

$$\frac{\Delta E}{Eu} \equiv \frac{V_1}{p_1}\left(q_1-\frac{\eta_1}{\bar{\eta}}\right)^2 = \frac{V_2}{p_2}\left(q_2-\frac{\eta_2}{\bar{\eta}u}\right)^2$$

and

$$\tau \equiv \frac{1}{p_1-p_2} = \frac{\eta_1}{p_1}\left(1-V_1\frac{\eta_1}{\bar{\eta}}\right) = -\frac{\eta_2}{p_2}\left(1-V_2\frac{\eta_2}{\bar{\eta}}\right)$$

Vi is the volume fraction of phase i; ηi is the viscosity of phase i undergoing Newtonian viscous flow, $\bar{\eta} \equiv V_1\eta_1 + V_2\eta_2$; qi is the phase 'stress-concentration' factor, $V_1q_1 + V_2q_2 = 1$; pi is internal stress caused by the mismatch in creep strains between the phases, $V_1p_1 + V_2p_2 = 0$.

The Eqn. (5) is also valid for the case wherein one of the phases is nondeformable by creep if diffusional mass transport around the purely elastic phase is taken into account.

2.2. Theoretical models for plastic deformation

There are several theoretical models for creep deformation. In general, they can be divided into two broad categories: boundary mechanisms [5–11] and lattice mechanisms [5,12]. Boundary mechanisms rely on the presence of grain boundaries and occur only in polycrystalline materials. They are associated with some dependence on grain size so that $p \geqslant 1$. Lattice mechanisms are independent of the presence of grain boundaries and occur both in single crystal and polycrystalline materials. They occur within the grain interiors and are independent of grain size, so $p = 0$.

The boundary mechanisms can be subdivided into four categories: diffusion creep, [5–7] interface reaction controlled diffusion creep [8], grain boundary sliding and grain rearrangement [5,6,9,10], and cavitation creep and microcracking [11]. In diffusion creep where vacancies may flow from the zones experiencing tension to those in compression either through the crystalline lattice (Nabarro–Herring creep) or along the grain boundaries (Coble creep), the individual grains become elongated along the tensile axis Fig. 1). When grain boundaries do not act as perfect sources or sinks for vacancies, the process of creating or annihilating point

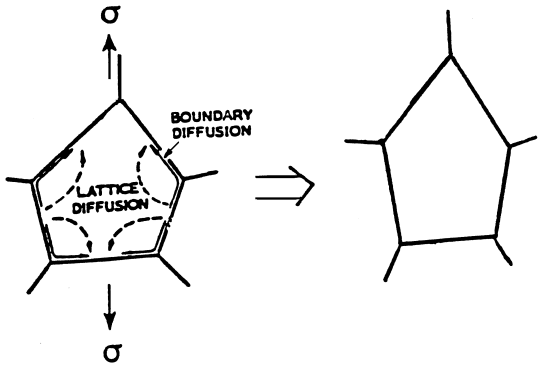

Fig. 1. Diffusion flow by lattice (Nabarro–Herring creep) or by grain boundaries (Coble creep).

defects may control the creep deformation. This is termed interface reaction-controlled diffusion creep. Because this process involves diffusion of vacancies, the grains are also elongated along the tensile axis. In grain boundary sliding and grain rearrangement, there are several different models (Lifshitz sliding, Rachinger sliding, Ashby and Verrall model, Gifkins model, etc.). Lifshitz sliding occurs naturally as part of diffusion creep, to maintain grain contiguity, the grains elongate along the tensile axis and maintain their adjacent neighbours, so there is no increase in the number of grains lying along the tensile axis. In contrast, during Rachinger sliding, the grains slide, rearrange and retain their original shapes, but exchange their neighbours, so there is an increase in number of grains along the tensile axis. In Ashby and Verrall model, which is two-dimensional, during the deformation process, grains suffer a transient but complex shape change by diffusional transport Fig. 2). While in the Gifkins model, which may be viewed as three-dimensional, during the deformation process, grains move apart by grain boundary sliding caused by the motion of grain boundary dislocations, resulting in a gap between the grains. When the gap is large enough, it is filled by an emerging grain from one layer to the next (Fig. 3) [10]. In these two models, the grains almost retain their original shapes, and there is an increase in number of grains along the tensile axis. In the cavitation creep and microcracking, extensive cavities form. They grow and link up forming microcrack by grain boundary sliding. The principal mode of deformation is a damage mechanism. Variations or refinements of the previous basic models have also been proposed by a number of authors but are not to be reviewed here.

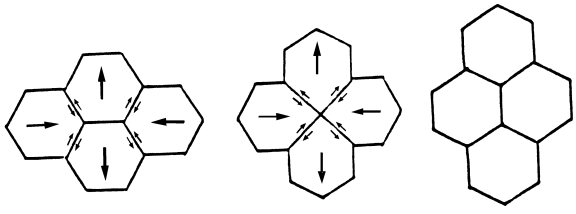

Fig. 2. Grain boundary sliding and grain rearrangement by diffusion (Ashby and Verrall model) [10].

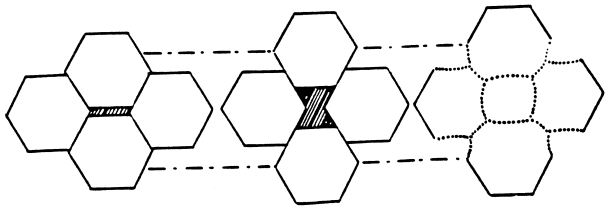

Fig. 3. Grain boundary sliding and grain rearrangement. A gap forms between four grains and is filled by an emerging grain (Gifkins model) [10].

The lattice mechanisms can be briefly subdivided into two categories [12]: dislocation climb and glide controlled by climb on the one hand and dislocation climb on the other (Fig. 4). For the dislocation climb and glide controlled by climb mechanism, in ceramics, the anion/cation ratio ra/rc is < 2, and the ceramics must have five independent slip systems. While for the dislocation climb from Bardeen–Herring sources, the ra/rc ratio is > 2, and the ceramics are either lacking some slip systems, or if five independent systems are available, not all may be active simultaneously [12]. The dislocation creep mechanisms involve the elongation of grains along the tensile axis as well.

2.3. Methods to identify deformation mechanism

In general, several mechanisms may contribute to the creep deformation at elevated temperature, but creep is usually controlled by only one of these mechanisms. To identify which mechanism is dominant, there are several methods.

Ashby [13] constructed deformation-mechanism maps by using rate-equations and sufficient data on the materials. These maps for example show the fields of stress and temperature in which each independent mechanism for plastic deformation is dominant. Knowledge of any two of the three variables (stress, temperature and strain-rate) locates a point on the map, identifies the dominant mechanism or mechanisms and gives the value of the third variable. Mohamed and Langdon [14] constructed deformation-mechanism maps with grain size as a variable. Based on the deformation-mechanism maps constructed by Ashby and Mohamed et al., Heuer et al. [9], for example, have devised a stress-grain size deformation mechanism map for MgO-doped Al_2O_3 at 1500°C (Fig. 5). They suggested that diffusional deformation dominated for most grain sizes of interest, but

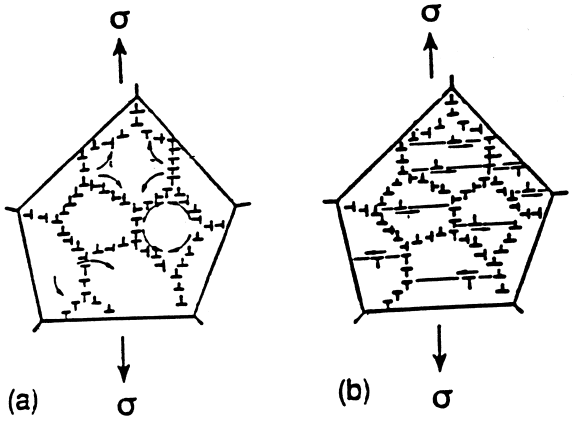

Fig. 4. Dislocations move by (a) climb, (b) climb and glide.

some basal slip could easily occur. Furthermore, when grain size of Al_2O_3 was between 50 and 500 μm and the imposed stress was large enough, then dislocation climb and glide could occur. But in practice, the theory and the experimental data used to construct the maps are poor or insufficient for many ceramic materials, thus limiting their use in applications.

At present, the main method to identify the possible rate controlling mechanism is to compare the values of n,p and Q obtained from experiments with theoretical predictions. Chokshi et al. [12] indicated that many ceramics exhibit stress exponents of ~5, ~3 or ~1, which appeared to be associated with dislocation glide and climb, climb from Bardeen–Herring sources, and diffusion creep, respectively. The stress exponent of ~2 might be due to the presence of a partially wetting grain boundary glassy phase or to control by an interface reaction. [12] Besides, the stress exponent between 1 and 3 might be associated with grain boundary sliding and grain rearrangement, and a higher stress exponent ($n \geqslant 3$) can also be associated with cavitation creep and microcracking. The inverse grain size exponent points to either a boundary mechanism ($p \geqslant 1$) or a lattice mechanism ($p = 0$). In general, a direct observation and analysis of the microstructure of the specimens after deformation is necessary to check preliminary conclusions drawn from the experimentally determined stress–strain rate relationships.

For two phase composites, especially for those with duplex microstructures, authors are not only interested in the dominant mechanism of deformation, but also try to find out which phase controls the creep behaviour. Creep of composites can be modelled by using standard composite theory: isostrain and isostress model [15,16] (Fig. 6). Isostrain and isostress prediction diagrams can be constructed by calculation. By comparing the experimental data with the isostrain and isostress prediction, the model fitting the creep deformation can be determined. Since the isostress model is dominated by the least creep resistant phase and highest creep rate and the isostrain model is dominated by the most creep resistant phase and lowest creep rate, the phase controlling the creep behaviour can be determined.

For the two phase composites in which both phases deform inelastically, a self-consistent model was developed [17,18], which predicts the deformation behaviour of the composites when the viscoplastic laws of each phase are known. By self-consistent calculations, effective strain rate sensitivity parameter and effective prefactor which are characteristic of the composite behaviour can be obtained. Stress and strain rates in each phase are also attainable. From the comparison between the model and the experiments, the possible deformation mechanisms of each phase can be determined and the phase controlling the creep behaviour can also be qualitatively determined.

3. Plastic deformation behaviours of Al_2O_3-based ceramic composites

In studies of the plastic deformation behaviours of Al_2O_3-based ceramic composites, great attention is concentrated on three aspects: strain rates, microstructural changes and deformation mechanisms.

As concerns the first of these items, one of the main aims is to investigate the relationship between the creep rates and operating variables (imposed stress, grain size, temperature) and to evaluate the creep parameters (n, p, Q). The deformation behaviours are critically dependent

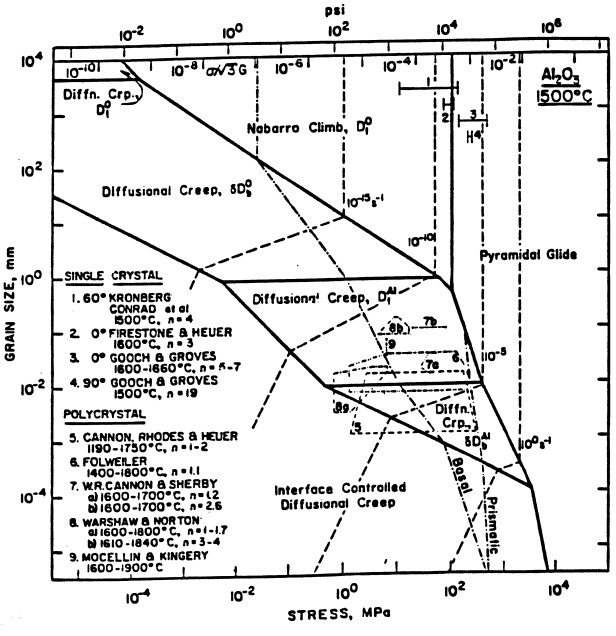

Fig. 5. Deformation map for MgO-doped Al_2O_3 at 1500°C [9].

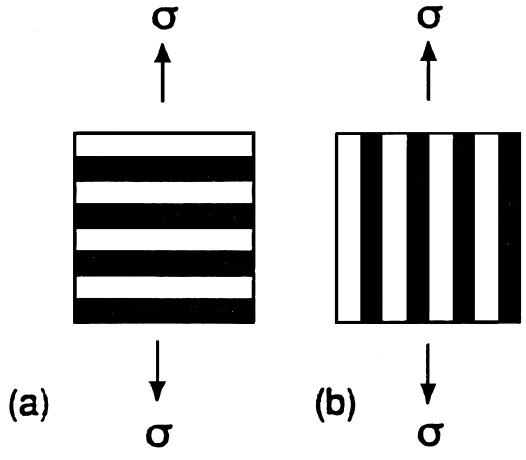

Fig. 6. Idealized composite microstructures: (a) isostress and (b) isostrain orientations.

on the physical and chemical properties of reinforcing particles or whiskers, their content, morphologies and distributions, and microstructures of composites including grain sizes and shapes, pores, grain boundaries, interfaces, as well as stress and temperature. During deformation, there often occur microstructural changes such as grain growth, changes of grain shape (grain elongation), texture development, formation of intermediate or intergranular phase, dislocation activity, vacancy nucleation and evolution, cavitation and evolution, formation and development of microcracks, etc. The study of such microstructural changes accompanying creep deformation is an essential aspect which is an important foundation for analysing creep deformation behaviours and creep mechanisms of composites.

In this chapter, we will first recall briefly the high temperature deformation behaviours of fine-grained alumina and then review the high temperature deformation behaviours of Al_2O_3-based ceramic composites.

High temperature deformation behaviours of fine-grained alumina were widely investigated. [5–9] [18–23] Most authors have shown that $n = 1$–2, $p = 2$–3, and $Q = 430$–$500\,\mathrm{KJ\,mol^{-1}}$ can represent deformation data at lower stress range. The stress exponent generally decreased with increasing grain size. In some studies, non-steady state deformation has been reported due to grain growth or cavitation. Fridez [21] has reported that creep deformation accelerated grain growth. The change in the crystallographic texture of alumina was observed at higher stress range. [21,23] The main deformation mechanisms were diffusional creep, grain boundary sliding and sometimes basal slip. The diffusional creep can become interface-controlled at low stresses, causing non-Newtonian creep behaviour. The cavitation was often caused by unaccommodated GBS or basal slip and the basal slip can give rise to a deformation texture.

In Al_2O_3-based ceramic particle or whisker composites, the creep behaviours of Al_2O_3-ZrO_2 and Al_2O_3-SiC composites have been most extensively investigated. In the following the creep behaviours of Al_2O_3-based oxide ceramic composites and Al_2O_3-based nonoxide ceramic composites will be discussed. The corresponding experimental data produced during the past 10 years or so in both families of materials are summarised in Tables 1 and 2, respectively.

3.1. Al_2O_3-based oxide ceramic particle composites

3.1.1. Al_2O_3-ZrO_2 composites

Since Wakai et al. reported that a 3 mol% yttria stabilized zirconia exhibited superplasticity [24], Al_2O_3-ZrO_2

Table 1
Deformation behaviours of Al_2O_3-based oxide ceramic particle composites

Reference	Additive	Content (vol%)	Test type [a]	Atm.	σ ranges (MPa)	ϵ ranges (S^{-1})	T (°C)	Grain size (μm) Al_2O_3	Grain size (μm) additive	n	p	Q ($\mathrm{KJ\,mol^{-1}}$)
Wakai et al. (1986) [25]	ZrO_2	72.7	C	air	–	10^{-4}–10^{-3}	1400–1500	–	–	1.2–2.0	–	620
Kellett et al. (1986) [26]	ZrO_2	20	C	air	30–100	10^{-4}–10^{-2}	1500	1.1	0.7	2.1	–	–
Wakai et al. (1988) [27]	ZrO_2	14.3	T	air	10–100	10^{-8}–10^{-5}	1250–1450	1.0	0.5	1.7–2.1	–	750
Wakai et al. (1988) [28]	ZrO_2	72.7	T	air	10–140	10^{-7}–10^{-5}	1250–1450	0.5	0.5	2.1	–	590–600
Nieh et al. (1989) [29]	ZrO_2	72.7	T	vacuum	5–40	10^{-5}–10^{-2}	1450–1650	~0.5 [b]		2	–	–
Wakai et al. (1989) [30]	ZrO_2	50	T	air	2–100	10^{-7}–10^{-3}	1250–1450	0.6	0.5	2.1–2.4	–	720–780
	ZrO_2	30.8	T	air	2–100	10^{-7}–10^{-3}	1250–1450	1.0	0.6	1.9–2.4	–	680–740
	ZrO_2	14.3	T	air	2–100	10^{-7}–10^{-3}	1250–1450	1.0	0.5	1.7–2.1	–	640–760
Wang et al. (1991) [31]	ZrO_2	5	C	argon	5–200	10^{-5}–10^{-4}	1400–1500	2.8	–	–	3	630
	HfO_2	5	C	argon	5–200	10^{-5}–10^{-4}	1400–1500	2.7	–	–	3	685
	TiO_2	5	C	argon	5–60	10^{-5}–10^{-4}	1400–1500	3.8	–	–	2	570
Owen et al. (1994) [32]	ZrO_2	72.7	T	air	4–100	10^{-8}–10^{-3}	1327–1477	0.4	0.4	2.8	2.1	585
French et al. (1994) [15]	ZrO_2	50	T	air	35–75	10^{-8}–10^{-6}	1200–1350	~2.3		1.8	–	633
	YAG	50	T	air	35–75	10^{-8}–10^{-7}	1210–1350	~2.0		2.6	–	695
Calderon-Mereno et al. (1995) [33]	ZrO_2	5.5	C	air	10–150	10^{-8}–10^{-4}	1300–1450	4.7	–	1.4	–	580
Calderon-Mereno et al. (1995) [33]	ZrO_2	5.5	C	air	10–150	10^{-8}–10^{-4}	1300–1450	2.6	< 1	1.8	–	540
Chevalier et al. (1997) [34]	ZrO_2	10	B	air	50–200	10^{-8}–10^{-6}	1200–1400	2	0.5	2.5	–	760
Calderon-Mereno (1997) [35]	ZrO_2	40	C	air	45–85	10^{-5}–10^{-4}	1400–1500	2.3	1.6	1.7	–	–
Calderon-Mereno (1997) [35]	ZrO_2	20	C	air	64–95	10^{-5}–10^{-4}	1500	2.3	1.6	1.4	–	–
Calderon-Mereno (1997) [35]	ZrO_2	10	C	air	70–123	10^{-5}–10^{-4}	1500	2.3	1.6	1.2	–	–
Flacher et al. (1997) [36]	ZrO_2	5–20	C	air	20–130	10^{-5}–10^{-4}	1300–1400	0.2̃		2	–	650
Clarisse et al. (1997) [37]	ZrO_2	80	C	air	4–200	10^{-6}–10^{-3}	1275–1400	0.64	0.55	1–2	–	640–705
Clarisse et al. (1997) [37]	ZrO_2	80	C	air	4–200	10^{-7}–10^{-3}	1275–1400	1.12	0.80	1–2	–	642–723
Clarisse et al. (1997) [37]	ZrO_2	80	C	air	4–200	10^{-7}–10^{-4}	1275–1400	1.40	0.71	1–2	–	663–715
Duong et al. (1993) [16]	YAG	50	C	air	3–20	10^{-8}–10^{-5}	1400–1500	10	3	1.1	–	612
	YAG	75	C	air	3–20	10^{-8}–10^{-5}	1400–1500	8	3	1.1	–	592

[a] C = compression, T = tension, B = bending.
[b] Average grain size.

composites have been extensively studied [15, 25–40]. Wakai and Kano [28] demonstrated that a 3 mol% yttria stabilized zirconia with 27.3 vol% alumina composite (3Y20A) was capable of large superplastic elongations of more than 200%, while Nieh et al. [29] reported a tensile elongation of 500% at 1650°C for 3Y20A. The superplasticity of the Al_2O_3-ZrO_2 composites has been reported by many other ceramic workers.

Inspection of all the available data of the Al_2O_3-ZrO_2 composites shown in Table 1 indicates that the values of n range from about 1.5 to 2.5. The activation energies tend to lie in the range 600–700 KJ mol^{-1}. The values of inverse grain size exponent were only reported by Wang et al. [31] and Owen et al. [23] ($p=3$, for 5 vol% ZrO_2; $p=2.1$ for 3Y20A). The differences in the values of n, Q and p are probably caused by the conditions of test, the different stress, strain rate and temperature ranges, the ZrO_2 content, the levels of impurities, and the microstructure of the composites.

Most studies on Al_2O_3-ZrO_2 composites indicated that the introduction of ZrO_2 in Al_2O_3 made the creep rate of the composites lower than that of either of their single-phase constituents. [15,27] [30–39] Wakai et al. [27,30] and Chen [39] attributed it to the suppression of interface reactions controlled diffusion creep of Al_2O_3 or hindrance of grain-boundary movement by intergranular ZrO_2 particles. French et al. [15] indicated that the decrease of the creep rate was caused by a strong segregation of Y^{3+} (and possibly Zr^{4+}) to the alumina grain boundaries, which resulted in a decrease of Al_2O_3 in grain boundary dislocation mobility and interface reaction controlling diffusional creep rate. The effect of ZrO_2 content on the creep rate of composites was first studied by Wakai et al. [30,38] (Fig. 7). The results showed that when the ZrO_2 content was more than 14.3 vol% the creep rate decreased with decrease of the ZrO_2 content. The values of n remained almost unchanged. Recent investigations [35–37] showed

Table 2
Deformation behaviours of Al_2O_3-based non-oxide ceramic particle or whisker composites

Reference	Additive	Content (vol %)	Test type	Atm.	σ ranges (MPa)	ϵ ranges (S^{-1})	T (°C)	Grain size (μm) Al_2O_3	additive	n	p	Q (KJ mol^{-1})
Chokshi et al. (1985) [41]	$SiC_{(w)}$[a]	18	B	air	40–100	10^{-7}–10^{-4}	1500	$\leqslant 5$	–	5.2	–	–
Porter et al. (1987) [42]	$SiC_{(w)}$	5–20	B	air	40–200	10^{-7}–10^{-3}	1450–1600	–	–	5	–	450
Lipetzky et al. (1988) [43]	$SiC_{(w)}$	33	B	air	30–250	10^{-10}–10^{-5}	1200–1300	1–2	–	1,5	–	450–500
Xia et al.	$SiC_{(w)}$	9.3,18	B	air	40–200	10^{-7}–10^{-4}	1400–1550	1–2	–	3.8	–	–
(1988) [44]	$SiC_{(w)}$	30	B	air	40–200	10^{-7}–10^{-4}	1400–1550	1–2	–	6.3	–	–
Lin et al.	$SiC_{(w)}$	20	B	air	37–300	10^{-9}–10^{-5}	1200–1400	2	–	2	–	–
(1990) [45]	$SiC_{(w)}$	20	B	air	>125	10^{-9}–10^{-5}	1400	2	–	7–8	–	–
DeArellano-Lopez et al. (1990) [46]	$SiC_{(w)}$	6–30	C	argon, air	100–300	10^{-8}–10^{-4}	1300–1500	–	–	1.2–1.8	–	620
Lin et al.	$SiC_{(w)}$	30–50	B	air	37–300	10^{-9}–10^{-5}	1300	1-2	–	6	–	–
(1991) [47]	$SiC_{(w)}$	30–50	B	air	37–300	10^{-9}–10^{-5}	1200	1-2	–	3	–	–
	$SiC_{(w)}$	10	B	air	37–300	10^{-9}–10^{-6}	1300	8	–	4	–	–
	$SiC_{(w)}$	10	B	air	37–300	10^{-9}–10^{-6}	1200	8	–	2	–	–
Lipetzky et al.	$SiC_{(w)}$	33	C	air	25–250	10^{-9}–10^{-6}	1200–1400	1–2	–	1,3	–	269, 655
(1991) [48]	$SiC_{(w)}$	33	C	nitrogen	25–250	10^{-9}–10^{-6}	1200–1400	1–2	–	1,3	–	210, 966
Swan et al. (1992) [49]	$SiC_{(w)}$	30	C	air	25–200	10^{-8}–10^{-5}	1200–1350	1–2	–	1.4–1.7	–	370
DeArellano-Lopez	$SiC_{(w)}$	5–30	C	argon	10–240	10^{-7}–10^{-5}	0491400	–	–	0.9–1.9	–	–
et al. (1993) [50]	$SiC_{(w)}$	15–30	C	argon	80–410	10^{-6}–10^{-4}	0491400	–	–	2.4–5.9	–	–
Xia et al. (1995) [51]	$SiC_{(w)}$	9.3	B	air	10–100	10^{-7}–10^{-4}	1400–1550	1–2	–	3.8	–	820–830
Lin et al.	$SiC_{(w)}$	10	B	air	50–230	10^{-8}–10^{-7}	1200	1.2–8	–	2	1	–
(1996) [52]	$SiC_{(w)}$	10	B	air	50–230	10^{-8}–10^{-7}	1300	1.2–8	–	3.5	–	–
Ohji et al.	$SiC_{(p)}$	17	T	air	50–150	10^{-10}–10^{-7}	1200–1300	2	0.1	3.1	–	–
(1994) [53]	$SiC_{(p)}$	17	B	air	100–200	10^{-11}–10^{-9}	1200	2	0.1	2.2	–	–
Deng et al.	$SiC_{(p)}$	10	B	air	40–125	10^{-9}–10^{-5}	1160–1400	<5	0.6	4.27	–	444
(1996) [54]	$SiC_{(p)}$	10	B	air	40–125	10^{-9}–10^{-5}	1160–1400	$\geqslant 5$	2.7	4.75	–	666
Katsumura et al. (1987) [55]	$TiC_{0.5}N_{0.5(p)}$	54	B	argon	50–300	10^{-6}–10^{-3}	1300–1400	0.8	1.4	2.0–2.2	–	281.5
Nagano et al. (1991) [56]	$TiC_{(p)}$	26	T	vacuum	8–70	10^{-5}–10^{-2}	1300–1550	1.2		3.2–4.1	–	853

[a] : $_{(w)}$ = whiskers, $_{(p)}$ = particles

almost the same results as those obtained by Wakai et al. But the results obtained by Clarisse et al. [37] showed that when ZrO_2 content exceeded that of Al_2O_3, the creep rate of the composites was somewhat higher than that of single-phase Al_2O_3 due to a more ductile ZrO_2 phase which played a role in the deformation of the composites. The values of n obtained by Calderon–Moreno [35] showed a slight increase with the ZrO_2 content.

Wang et al. [31] and Owen et al. [32] studied the influence of grain size on the creep behaviours of Al_2O_3–ZrO_2 composites. The values of p obtained by Wang et al. was about 3, while that obtained by Owen et al. was 2.1. The difference of the values of p is mainly caused by the content of ZrO_2. In the experiment of Wang et al. the ZrO_2 content was 5 vol%, but in the experiment of Owen et al. the ZrO_2 content was 72.7 vol%, and in this two phase composite the values of p of ZrO_2, Al_2O_3 phase and their volume average obtained by Owen et al. were 2.0, 2.6 and 2.1 respectively (Fig. 8). So, the addition of ZrO_2 decreases the values of p of Al_2O_3–ZrO_2 composites. The influence of grain size on the creep behaviours was also investigated by other authors [33,34,37]. The impurity content of Al_2O_3 and ZrO_2 and the level of segregation at grain boundaries may affect strongly the creep behaviours of the composites. Generally, the higher the content of Si, Fe, Na impurity, the higher the creep rate of the composite. Although French et al. [15] indicated that in Al_2O_3/c-ZrO_2 (8 mol% Y_2O_3) composite the segregation of Y^{3+} to the Al_2O_3 grain boundaries slowed the creep rate of this composite, the results obtained by Chevalier et al. [34] showed that magnesia-stabilized ZrO_2-Al_2O_3 composite decreased the creep rate while yttria-stabilised zirconia was not favourable for creep resistance of the composite. The authors suggested that a magnesium-containing grain boundary glassy phase was favourable for creep resistance of the composite. The role of the Y^{3+} and Mg^{2+} at grain boundaries needs to be more systematically investigated.

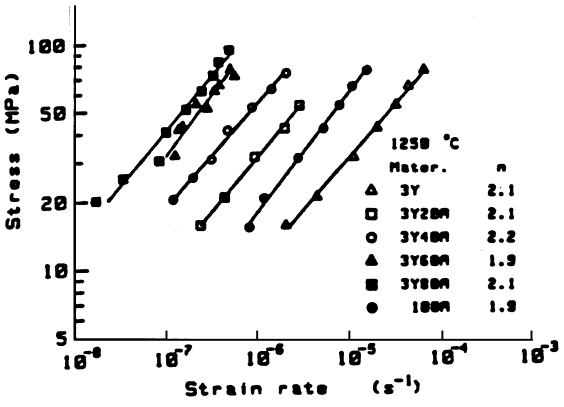

Fig. 7. Influence of ZrO_2 content on the strain rate in Al_2O_3-ZrO_2 composites [38].

Microstructural characterization of the deformed specimens generally revealed remarkable structural stability as long as the second phase was present at a small volume fraction, typically no more than 10% [2]. Chen attributed this to the particle pinning effect [2]. The measurements showed that there was no or very limited concurrent grain growth during deformation [15,28,29,32,33] and there was no significant change in the aspect ratio of the grains, which essentially retained their equiaxed shapes [29,33]. Wakai et al. [28] and Owen et al. [32] observed that in 3Y20A there was very little increase in the aspect ratio of the two phases following deformation, the grains were elongated slightly in the tensile direction. The grain aspect ratio of ZrO_2 grains was 1.15–1.16, and that of Al_2O_3 grains was 1.3–1.5. This implies that the intragranular strain of ZrO_2 grains is smaller than that of Al_2O_3 grains. In some experiments, neither significant intragranular dislocation activity nor significant cavitation was observed [15,32], but in most experiments, cavitation was noted [28,33,34]. Cavities tended to nucleate at triple point junctions associated with an alumina grain and then they grew quite quickly along those Al_2O_3–Al_2O_3, ZrO_2–ZrO_2 and Al_2O_3–ZrO_2 interfaces normal to the tensile axis. The cavity volume fraction and size were dependent on the strain rate, both decreasing with decreasing strain rate.

Many authors ruled out the deformation mechanisms of intragranular dislocation or significant contributions

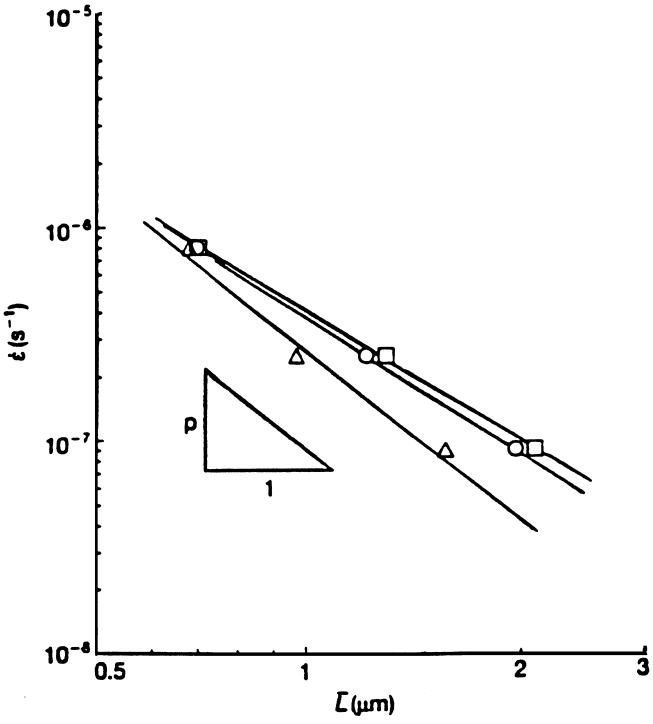

Fig. 8. Variation in creep rate with grain size for Al_2O_3–72.7 vol% ZrO_2 composite. The grain size may be defined in terms of the ZrO_2, or Al_2O_3 phases or their volume average. p: (□) ZrO_2, 2.0; (Δ) Al_2O_3, 2.6; (o) Av. 2.1 [32].

from diffusion creep by comparison of the stress exponent with theoretical predictions and the observation of microstructures of Al_2O_3–ZrO_2 composites. They attributed the deformation to some form of grain boundary sliding and grain rearrangement process [27–29,32–37]. Owen et al. indicated that in their study of 3Y20A the grain boundary sliding was mostly of the Rachinger type [32]. Calderon–Moreno et al. pointed out that grain boundary sliding with a mix of IRC (interface–reaction controlled) and TMC (transport of matter controlled) was the main deformation mechanism in their study [33]. Wakai et al. [30] indicated that when the content of ZrO_2 was very small and the size of ZrO_2 grains was much smaller than that of Al_2O_3 grains, the interface–reaction controlled diffusion creep could be the main creep mechanism. Clarisse et al. proposed that the main mechanism was grain boundary sliding accommodated by either grain boundary diffusion at high stress or an interface reaction at low stress in their study [37]. While in the study of Chevalier et al. [34], it is proposed that cavitation and microcracking by grain boundary sliding was the main mechanism. This is possibly related to their type of test (bending) and higher effective stresses.

From those investigations mentioned above, it can be seen that the introduction of ZrO_2 in Al_2O_3 can improve the creep resistance of Al_2O_3 matrix either by the suppression of interface reactions controlled diffusion creep of Al_2O_3 or by the hindrance of grain-boundary movement. In some conditions, the creep rate increases but the value of n remains almost unchanged or increases slightly with increasing the ZrO_2 content. The addition of ZrO_2 can decrease the values of p of Al_2O_3–ZrO_2 composites. The impurities of Si, Fe, Na at grain boundaries favour grain boundary sliding, a higher level of such impurities results in a higher creep rate of the composite. But the effect of Y^{3+} or Mg^{2+} on the creep rate of the composites is ambiguous, further investigation is needed. Microstructures of the composites show considerable stability due to the ZrO_2 particle pinning effect and there is no or very limited concurrent grain growth during deformation. Cavitation caused by unaccommodated grain boundary sliding often occurs during deformation. The main creep mechanism is grain boundary sliding and grain rearrangement.

3.1.2. Al_2O_3-$Y_3Al_5O_{12}$ composites

The studies of the creep behaviour of the Al_2O_3–$Y_3Al_5O_{12}$ system showed that the strain rate of the composites was lower than for pure Al_2O_3 or $Y_3Al_5O_{12}$ [15,16] (Fig. 9). French et al. attributed it to the strong segregation of Y^{3+} to interfaces hindering interface reaction controlling diffusional rate [15]. Duong et al. indicated that the creep rate was controlled by the $Y_3Al_5O_{12}$ phase which is more creep-resistant. [16] The values of n and Q obtained by French et al. were 2.6,

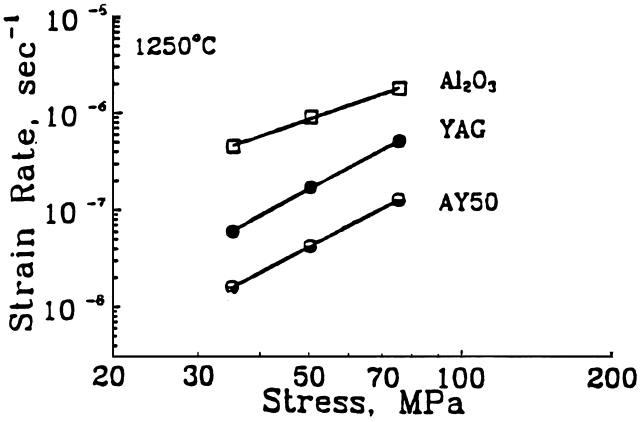

Fig. 9. Variation in strain rate with stress for Al_2O_3, $Y_3Al_5O_{12}$ and Al_2O_3-50 vol% $Y_3Al_5O_{12}$ composite [15].

695 KJ mol^{-1}, respectively. While those obtained by Duong et al. were 1.1, 612 KJ mol^{-1}, respectively. The difference is possibly caused by different test types and range of applied stress. The formers performed their tests under tension at higher stress (25–75 MPa), while the latter's tests under uniaxial compression at lower stress (3–20 MPa). The experiments of Duong et al. showed that the grain size rather than $Y_3Al_5O_{12}$ content played an important role in the creep behaviour, and the value of the stress exponent was independent of temperature.

The observation of microstructure of the Al_2O_3–$Y_3Al_5O_{12}$ composites showed that no dynamic grain growth occurred as a result of the deformation. [15,16] The grains remained fairly equiaxed after deformation. The evidence of cavitation was observed by Duong et al., the amount of cavitation was estimated to be between 2 and 5% [16]. While French et al. did not observe significant cavitation. The former authors performed their tests at more elevated temperatures. Higher temperature may favour the nucleation and growth of cavities.

As far as the deformation mechanism is concerned, Duong et al. suggested that the creep behaviour was controlled by a diffusional Nabarro–Herring mechanism [16]. French et al. proposed a diffusional creep controlled by an interface reaction (source–controlled) mechanism. [15] The creep data correlated well with the predicted behaviour based on the isostress model [16]. Thus, the authors suggested that the creep behaviour was most probably controlled by $Y_3Al_5O_{12}$ in their conditions.

3.1.3. Al_2O_3–TiO_2 composite

A study of the creep behaviour of Al_2O_3–TiO_2 composite was reported by Wang et al. [31] The addition of 5 vol% TiO_2 into Al_2O_3 matrix obviously enhanced its creep rate. This composite exhibited excellent

superplastic properties because of its lower flow stress and stronger interfacial cohesion. The apparent activation energy was 570 KJ mol^{-1}, which is higher than that of Al_2O_3 (420 KJ mol^{-1}) obtained by the authors. The authors suggested that an increase in the boundary diffusion activation energy due to dopants was correlated to the corresponding decrease in the interfacial energy, that is the cohesion at the interface increased with the activation energy.

Observation of the influence of grain size on the creep behaviour showed that the addition of TiO_2 into Al_2O_3 made the values of p decrease from 3 to 2. This means that the addition of titanium increased the lattice cation vacancy concentration of Al_2O_3 matrix, so that the lattice diffusion of aluminium overtook boundary diffusion, thus resulting in the change of the values of p.

It must be pointed out that the Al_2O_3–TiO_2 composite shows a poor high temperature fluxural strength because titania forms a nearly continuous network of aluminium-titanate at the grain boundary in the as-sintered specimens and this compound deteriorates the fracture strength of the Al_2O_3–TiO_2 composite.

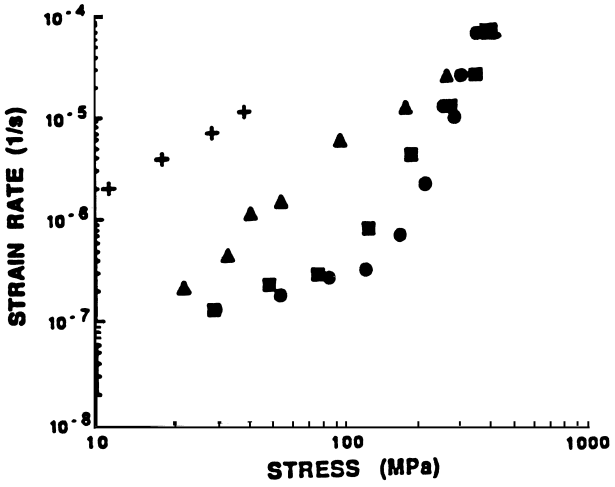

Fig. 10. Influence of stress on stress exponent in Al_2O_3-$SiC_{(w)}$ composites (+) SiC content: 0, 10–40 MPa, $n=1.3$; (▲) SiC content: 5, 20–240 MPa, $n=1.8$; (■) SiC content: 15, 30–80 MPa, $n=0.8$, 125–410 MPa, $n=3.4$; (●) SiC content: 30, 30–165 MPa, $n=0.9$, 170–370 MPa, $n=5.9$ [50].

3.2. *Al_2O_3–based non-oxide ceramic particle or whisker composites*

3.2.1. *Al_2O_3–$SiC_{(w)}$ composites*

Since the initial work on the creep behaviour of Al_2O_3–$SiC_{(w)}$ composites reported by Chokshi and Porter [41], many studies on such materials have been made. Generally the SiC whisker diameters were in the range 0.1 to 1 μm and their aspect ratio about 10–20.

Almost all the studies on Al_2O_3–$SiC_{(w)}$ composites (Table 2) have shown that their creep resistance was generally far superior to that of the unreinforced matrix [41–52]. The creep rate was found to be one or two orders of magnitude lower than that of Al_2O_3 matrix [45,49]. Most authors attributed the improvement in creep resistance to the whiskers which act as hard pinning particles on the grain boundary surfaces and as hard particles penetrating across the boundary planes, thus retarding creep deformation by grain boundary sliding [45–50,52].

Inspection of the values of the stress exponent of Al_2O_3–$SiC_{(w)}$ composites shown in Table 2 indicates that the values of n vary from 1 to 7–8, depending upon the method of test, the stress, temperature ranges, the $SiC_{(w)}$ content, and so on. The variation of the stress range often resulted in the change of the values of n [43,45,50]. From levels of about 1–2 at lower stresses, they increased to 5–7 at higher stresses (Fig. 10). This is attributed to a change in the creep mechanism. Higher stresses often lead to extensive cavitation occurring within glass pockets at interfaces and grain boundaries, and crack generation which causes matrix grains to separate from the whiskers, thus increasing the creep rate. DeArellano-Lopez et al. [50] introduced a critical stress level σ_c which depended on the content and impurities of whiskers, as well as the test conditions. When stresses were larger than σ_c, the stress exponent changed from its lower value to higher value. Higher content, higher purity of whiskers, lower impurity of the specimens and an inert atmosphere in tests might lead to a higher value of σ_c.

Experiments on the influence of temperature on the creep behaviours showed that a higher temperature often resulted in a higher value of n [41–48,51]. The stress exponents for Al_2O_3-33 vol% $SiC_{(w)}$ obtained by Lipetzky et al. changed from 1 at 1200°C to 3 at 1300–1400°C [48] (Fig. 11). The stress exponents for different content (10–50 vol%) $SiC_{(w)}$ composites obtained by Lin et al. varied from 2–3 at 1200°C to 3.5–6 at 1300°C. [45,47,52] Higher values of n (3.8–6.3) were also obtained by Chokshi et al., [41] Porter et al. [42] and Xia et al. [44,51]. Their experiments were all performed at higher temperatures (1400–1600°C) using four-point bending creep tests. Although the values of n obtained by DeArellano-Lopez et al. [46] and Swan et al. [49] using compression tests were lower (1–1.8), their results also showed that a higher temperature favoured a higher value of n. The increase of n at higher temperature is attributed to two factors: more extensive cavitation and crack caused by the stress concentrations resulted from thermal mismatch and more glassy phases at grain boundaries caused by the thermal oxidation of SiC whiskers.

The effect of the content of SiC whiskers on the creep behaviours was studied by some authors. When the whisker content was $\leqslant 20$ vol%, the creep resistance

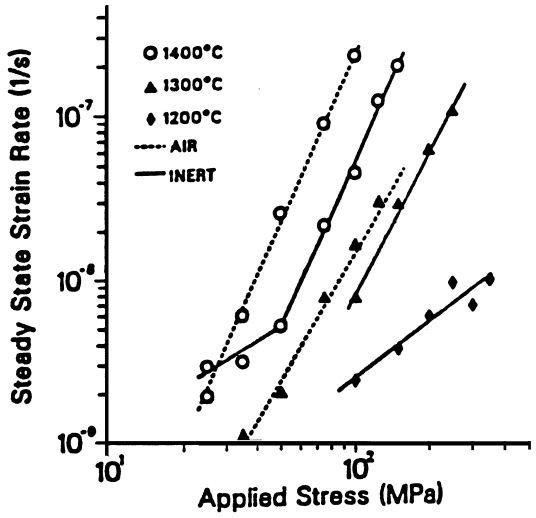

Fig. 11. Influence of temperature on stress exponent in an Al_2O_3–33 vol% $SiC_{(w)}$ composite (at 1200°C, $n=1$; at 1300, 1400°C, $n=3$) [48].

increased with increasing whisker content [42,46,47] and the values of n were lower [46,47], but when the whisker content exceeded 30 vol%, the creep rates and the values of n increased due to (1) the promotion of creep cavitation and crack generation from the higher number density of nucleation sites, and (2) more extensive formation of grain boundary glassy phase.

The effect of test ambient on creep behaviours is an important issue since the SiC whiskers are easily oxidized in air at elevated temperature. Experiments [46,48] showed that although the stress exponents were almost the same in different ambients, the creep rates were higher in air than in inert atmosphere. Lin et al. [52] have investigated the effect of matrix grain size (varying from 1.2 to 8.0 μm) on the creep behaviours. At 1200°C the creep rate exhibited an inverse grain size exponent of approximately 1, but at 1300°C the creep rate was not sensitive to the grain size due to enhanced nucleation and coalescence of creep cavities and the development of macroscopic cracks as the grain size increased. In addition, the creep rate of Al_2O_3–$SiC_{(w)}$ composites was accelerated by the introduction of certain additives (i.e. Y_2O_3) [47]. The presence of an intergranular glassy phase introduced by the Y_2O_3 additive facilitated creep deformation resulting in an order of magnitude increase in creep rate. Finally, it should be pointed out that the method of creep testing may also influence the experimental results. In four-point bending creep tests, the creep rate is strongly affected by the surface tensile properties of the specimens. The growth of surface cracks can result in a creep exponent of $\sim$2 or higher when the growth rate of microcrack obeys a power-law dependence on the local normal stress. This mode of testing can result in large errors in the stress exponent [49].

Microstructural observation of creep specimens generally revealed more or less cavitation at interfaces, grain boundaries and triple joint junctions. [43,45–50,52] Unaccommodated grain boundary sliding was considered to be responsible for the formation of cavities. Higher stresses and higher temperatures often increased the amount of intergranular voids, cavities and cracks, and sometimes caused the separation of interfaces and grain boundaries [43,48]. The Al_2O_3–$SiC_{(w)}$ composites exhibited higher number density and smaller cavities than those of monolithic Al_2O_3 [45]. One study showed that 30 and 50 vol% $SiC_{(w)}$ composites exhibited cavity number density 2 orders of magnitude higher than that of Al_2O_3-20 vol% $SiC_{(w)}$ composite. The average cavity size of 30 and 50 vol% $SiC_{(w)}$ composites was 0.4 μm, while that of 20 vol% composite was 0.05 μm [47]. In the four-point bending tests, the cavity number density was approximately 1 to 2 orders of magnitude in the compressive surface region less than that in the tensile surface region [47], and at higher temperature, cracklike cavities tended to form extensive macroscopic tensile surface cracks, and the number of surface cracks increased with the grain size of Al_2O_3 [52].

Although a glassy phase was present in very limited amounts in some as-sintered composites, many authors [43,46,47,49,52] observed that after creep deformation in air ambient a SiO_2–rich glassy phase around the whiskers had formed due to the oxidation of the latter. In most cases, the glassy phase penetrated along grain boundaries and interfaces and accumulated at triple grain junctions throughout the materials, which presumably facilitated grain boundary sliding and increased the creep rate.

Dislocation networks were observed by some authors [42,43,46,49,51]. But in most cases, the dislocation density was very low [42,43,46,49] and the dislocation networks were also observed in the as-sintered specimens. They probably formed as a result of the large residual stresses resulting from thermal expansion mismatch during the fabrication processing. Contrary to other authors, Xia et al. [51] observed extensive dislocation networks in the crept specimens, and higher dislocation densities were observed in specimens deformed to large strains.

Some authors observed the grain offset and rotation of Al_2O_3 [45,52]. As far as the creep mechanism is concerned, in early studies, a dislocation-controlled creep mechanism was proposed by some authors [41,42,44]. But no sufficient microstructural information was presented to support this assertion, and this mechanism for the deformed Al_2O_3–$SiC_{(w)}$ composites remains doubtful. A more recent study [51] revealed extensive dislocation activity and very little evidence for the development of initial cavitation. The authors proposed an intragranular dislocation mechanism controlled by lattice

diffusion of the oxygen anions. So, the dislocation-controlled creep mechanism can not be ruled out under some conditions (for example: lower $SiC_{(w)}$ contents and imposed stress levels, higher temperatures and strains).

A grain boundary sliding mechanism accommodated by diffusion to a larger or lesser extent was proposed by many authors [43,45–49,52]. Some experiments pointed to the existence of two stress-dependent plastic deformation mechanisms [43,45,47,50]. At low stress, grain boundary sliding controls the deformation, while at high stress, the creep deformation is controlled by creep cavitation and microcracking. Lipetzky et al. [43] proposed that at low stress levels the primary creep deformation mechanism was diffusional creep and grain boundary sliding facilitated by viscous flow of intergranular silica glass. Swan et al. [49] also indicated that the introduction of SiC whiskers into the matrix slowed the creep rate by diffusion and increased the amount of grain boundary sliding. The experiments of De Arellan-Lopez et al. [50] showed that when the $SiC_{(w)}$ content was < 15 vol%, the deformation was controlled by grain boundary sliding, but when the $SiC_{(w)}$ content was $\geqslant 15$ vol%, the whiskers impeded grain boundary sliding effectively, causing a change in the deformation mechanism to pure diffusional creep.

3.2.2. Al_2O_3–$SiC_{(p)}$ composites

Since SiC whiskers are expensive for practical applications and raise health hazards during material processing, Al_2O_3–SiC particle composites were developed more recently. Studies on their creep behaviours showed that these composites exhibited excellent resistance [53,54] as Al_2O_3–$SiC_{(w)}$ composites did. By dispersing 17 vol% SiC nanoparticles into Al_2O_3, creep life was 10 times longer, creep strain was 8 times smaller and creep rate was 3–4 orders lower than those of monolithic Al_2O_3 [53] (Fig. 12). The authors attributed it to rotating and plunging of intergranular SiC nanoparticles into Al_2O_3 grain which were observed on microstructures of deformed specimens such as strain contrast contours, small cavities around the SiC nanoparticles, curved grain boundaries of Al_2O_3, etc. Further study [55,56] revealed that SiC/Al_2O_3 interfaces possessed much stronger bonding than Al_2O_3/Al_2O_3 boundaries. The magnitude of interfacial fracture energy between SiC and Al_2O_3 was over twice the Al_2O_3/Al_2O_3 grain boundary fracture energy, i.e. grain boundary of Al_2O_3/SiC composite was strengthened by SiC nanoparticles due to the stronger interfaces. Deng et al. introduced 10 vol% of 2.7 μm SiC particles into Al_2O_3, and the creep rate was markedly decreased [54], Their observations of microstructure showed that, when SiC particles were irregular and elongated, and most of them were entrapped into Al_2O_3 matrix grains, the creep resistance of the composite was higher, but equiaxed SiC particles

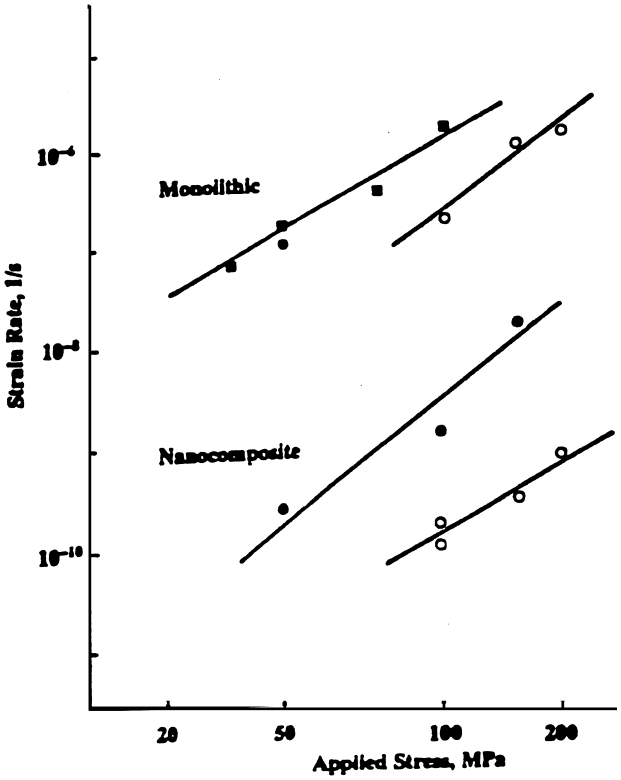

Fig. 12. Variation in strain rate with stress for Al_2O_3 and Al_2O_3–17 vol% SiC (p) nanocomposite (filled symbol: in the tension test; open symbol: in the flexture test) [53].

with most of them lying at the grain boundaries or triple-grain junctions did not increase the creep resistance. The authors attributed it to the serious oxidation of SiC particles on the grain boundaries. The presence of a viscous amorphous film decreased the interface bond strength and decreased the creep resistance [54].

The creep mechanism of Al_2O_3–SiC (p) composites was proposed to be grain boundary sliding more or less fully accommodated by diffusion as that of Al_2O_3–$SiC_{(w)}$ composites.

From the above, the deformation behaviours of Al_2O_3–SiC composites can be briefly summarized as follows:

The introduction of SiC into Al_2O_3 increases the creep resistance of composites to about one or two orders of magnitude superior to that of Al_2O_3 matrix, resulting from the pinning or penetrating role of the SiC whiskers or particles at grain boundaries. The creep resistance of the composites increase with increasing SiC content, but too high a SiC content is unfavourable to the creep resistance. Higher temperatures and higher stresses often result in both a higher value of n and a higher creep rate due to more extensive cavitation and microcracks caused by the stress concentration. The SiC whiskers or particles are easily oxidised in air at elevated temperatures, forming grain boundary glassy phase

containing SiO2 which decreases the creep resistance. Impurities such as Y_2O_3 favour the formation of the grain boundary glassy phase as well. Unaccommodated grain boundary sliding often causes cavitation and microcracks. In some conditions, dislocation creep causes dislocation networks. The main creep mechanism of the Al_2O_3–SiC composites is grain boundary sliding some accommodated by diffusion and some unaccommodated in most instances. But in some instances, a creep cavitation and microcracking mechanism or a dislocation creep mechanism may control the deformation of the composites.

3.2.3. Al_2O_3–TiC_xN_{1-x} composites

Although the processing of Al_2O_3–TiC_xN_{1-x} composites ($x = 0$–1) has been known for some time and their ambient temperature mechanical properties were reported, their high temperature mechanical properties, especially the creep behaviours, remain but poorly documented.

Nagano et al. [57] studied the deformation of Al_2O_3-26 vol% TiC composite. Their experiments showed that this Al_2O_3–TiC composite exhibited a ductility of 66% in tension. It deformed at a faster strain rate than Al_2O_3 in the high stress region. The values of the stress exponent increased with increasing temperature, from 3.2 (at 1450°C) to 4.2 (at 1550°C), respectively (Fig. 13). The authors suggested that the difference in stress exponent might be affected by the stoichiometry of TiC itself modified by reaction between TiC and Al_2O_3. The grain shape after deformation was changed. The grain aspect ratio was 1.26 in the direction of tensile stress. Cavities were also observed at grain boundaries. No new phase was found at temperatures lower than 1500°C, but Ti2O3 formed by the reaction between Al_2O_3 and TiC was observed in the specimens tested at 1550°C. The Ti_2O_3 phase developing at grain boundaries led to increased strain rates. The creep deformation of the Al_2O_3–TiC composite was mainly attributed to grain boundary sliding although the diffusion of Al_2O_3 and dislocation motion controlled by the diffusion of carbon of TiC played a small part in the deformation of the composite.

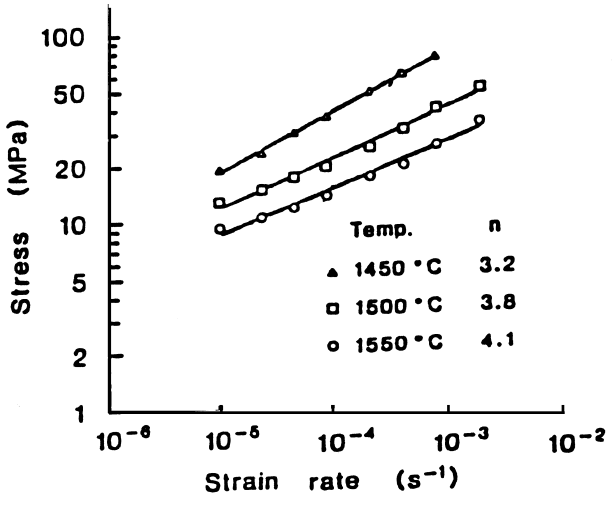

Fig. 13. . Influence of temperature on stress exponent in an Al_2O_3–TiC composite [56].

The deformation in Al_2O_3-54 vol% $TiC_{0.5}N_{0.5}$ composite was studied by Katsumura et al. [58]. This material showed higher strength at elevated temperature. It deformed above 1300°C and exhibited a superplastic behaviour. The values of n were almost unchanged with the temperature, 2.2 (at 1300°C) and 2.0 (at 1400°C), respectively. The apparent activation energy was rather low (281.6 KJ mol^{-1}). The observation of microstructure of the deformed specimens showed that the grain size was nearly the same as that before deformation and the grains remained equiaxed. No new phase was formed. Furthermore, the authors observed that the amount of $TiC_{0.5}N_{0.5}$ grains in the deformed section was slightly less than that of $TiC_{0.5}N_{0.5}$ grains in the undeformed section. They suggested the migration of Al_2O_3 against $TiC_{0.5}N_{0.5}$ during the deformation and proposed a 'heterogeneous grain boundary sliding' mechanism in this composite. This conclusion however should be verified by more microstructural information.

Jiao et al. [56] evaluated the interfacial fracture energy and its relation to mechanical behaviour in Al_2O_3-5 wt% TiN nanocomposite. They pointed out that according to a theoretical calculation the interfacial fracture energy between TiN and Al_2O_3 was much higher than grain boundary fracture energy of Al_2O_3, but in fact, this composite was found to fracture intergranularly in a similar manner to monolithic Al_2O_3 and its strength was 35% less than that of Al_2O_3. This is presumably due to the formation of TiO_2 at Al_2O_3/TiN interfaces, resulting in a lower interfacial fracture energy and weaker grain boundaries of Al_2O_3, which deteriorate the high temperature mechanical properties including creep resistance of the Al_2O_3–TiN composite.

4. Summary

Since Al_2O_3-based ceramic composites possess excellent mechanical properties at moderate temperatures, their plastic deformation behaviours are also investigated in the purpose to evaluate their practical applications at high temperature. In this paper, creep mechanisms of ceramic materials are first briefly reviewed. Then the studies of plastic deformation behaviours of Al_2O_3-based ceramic particle or whisker composites since the mid 1980s are reviewed. The influences of various factors on the creep behaviours, the changes of the microstructure of the deformed specimens, and the creep mechanisms of the Al_2O_3-based ceramic composites are summarised and analysed.

In the Al_2O_3-based oxide ceramic particle composites, Al_2O_3–ZrO_2 composites have been extensively investigated. The addition of ZrO_2 in Al_2O_3 makes the creep resistance of the composites superior to either of their single-phase constituents. In certain conditions, the creep rate increases with increasing the ZrO_2 content. The impurities such as Si, Fe, Na at grain boundaries favour grain boundary sliding, thus increasing the creep rate. The effect of Y^{3+} or Mg^{2+} on the creep rate of the Al_2O_3–ZrO_2 composites is ambiguous and needs to be further investigated. Microstructures of deformed specimens of Al_2O_3–ZrO_2 composites show considerable stability. The main creep mechanism of Al_2O_3–ZrO_2 composites is grain boundary sliding and grain rearrangement.

Other Al_2O_3-based oxide ceramic particle composites such as Al_2O_3–$Y_3Al_5O_{12}$ composite show an excellent creep resistance. However, they are less documented and need more investigation.

In the Al_2O_3-based nonoxide ceramic particle or whisker composites, most studies concentrate on Al_2O_3–SiC composites, especially Al_2O_3–$SiC_{(w)}$. The introduction of SiC into Al_2O_3 strongly increases the creep resistance of the material. Higher temperatures and higher stresses often result in extensive cavitation and microcracks in Al_2O_3-$SiC_{(w)}$ composites, increasing their creep rate and resulting in a higher stress sensitivity. In air ambient, the oxidation of SiC whiskers or particles may greatly decrease the creep resistance. The main creep mechanism of the Al_2O_3-SiC composites is grain boundary sliding partially accommodated by diffusion. In some conditions the deformation may be controlled by a creep cavitation and microcracking mechanism or even by a dislocation creep mechanism.

Other Al_2O_3-based nonoxide ceramic composites, such as Al_2O_3–TiC, Al_2O_3–TiC_xN_{1-x}, Al_2O_3-TiN composite have been less investigated. During deformation of those composites, the existence of TiO_2 or Ti_2O_3 at grain boundaries or interfaces introduced by additives or formed by the reaction between Al_2O_3 and additives during the deformation deteriorates the high temperature strength and the creep resistance of the composites. Avoiding or controlling the existence of TiO_2 or Ti_2O_3 at grain boundaries or interfaces during the deformation will be an important future issue in this kind of composites.

References

[1] R. Raj, M.F. Ashby, On grain boundary sliding and diffusional creep, Metall. Trans. 2 (1971) 1113–1127.

[2] I.W. Chen, Superplastic ceramic composites, Ceram. Trans. 19 (1991) 695–706.

[3] K.S. Ravichandran, V. Seetharaman, Prediction of steady state creep behaviour of two phase composites, Acta Metall. Mater. 41 (1993) 3351–3361.

[4] K. Wakashima, Fubi. Liu, Unsteady diffusional creep of a dual-phase material, Scripta Mater. 36 (1997) 1081–1087.

[5] W.R. Cannon, O.D. Sherby, Creep behaviours and grain boundary sliding in polycrystalline Al_2O_3: Journal of the American Ceramics Society 60 (1977) 44–47.

[6] C.K. Davies, Ray S.F. Sinha, High temperature creep deformation of polycrystalline alumina in tension, in: P. Popper, (Ed.), Special Ceramics 5, British Ceramic Research Association, Stoke on Trent, UK, 1972, pp. 193–209.

[7] E.M. Passmore, T. Vassilos, Creep of dense, pure, fine grained aluminium oxide, Journal of the American Ceramics Society 49 (1966) 166–168.

[8] A.H. Chokshi, J.R. Porter, High temperature mechanical properties of single phase alumina, Journal Mater. Sci. 21 (1986) 705–710.

[9] A.H. Heuer, N.J. Tighe, R.M. Cannon, Plastic deformation of fine-grained alumina (Al_2O_3): II. Basal slip and non-accommodated grain-boundary sliding, Journal of the American Ceramics Society 63 (1980) 53–58.

[10] J.P. Poirier, in: P.H. Cook, W.B. Harland, N.F. Hughes, A. Putnis, J.G. Sclater, M.R.A. Thomson (Eds.), Cambridge University Press, Cambridge, 1985, pp. 194–212.

[11] D.R. Clarke, High temperature deformation of a polycrystalline alumina containing an intergranular glassy phase, Journal Mater. Sci. 20 (1985) 1321–1332.

[12] A.H. Chokshi, T.G. Langdon, Characteristics of creep deformation in ceramics, Mater. Sci. Technol. 7 (1991) 577–584.

[13] M.F. Ashby, A first report on deformation-mechanism maps, Acta Metall. 20 (1972) 887–897.

[14] F.A. Mohamed, T.G. Langdon, Deformation mechanism maps based on grain size, Metall. Trans. 5 (1974) 2339–2345.

[15] J.D. French, J. Zhao, M.P. Harmer, H.M. Chan, G.A. Miller, Creep of duplex microstructures, Journal of the American Ceramics Society 77 (1994) 2857–2865.

[16] H. Duong, J. Wolfenstine, Creep behaviour of fine-grained two-phase Al_2O_3–$Y_3Al_5O_{12}$ materials, Mater. Sci. Eng. A. A172 (1993) 173–179.

[17] I.W. Chen, A.S. Argon, Steady state power-low creep in heterogeneous alloys with coarse microstructures, Acta Metall. 27 (1979) 758–791.

[18] E. Herve, R. Dendievel, G. Bonnet, Steady-state power-low creep in inclusion matrix composite materials, Acta Metall. Mater. 43 (1995) 4027–4034.

[19] R.M. Canon, W.H. Rhodes, A.H. Heuer, Plastic deformation of fine-grained alumina (Al_2O_3): 1, Interface-controlled diffusional creep, Journal of the American Ceramics Society 63 (1980) 46–53.

[20] A.H. Chokshi, J.R. Porter, Analysis of concurrent grain growth during creep of polycrystalline alumina, Journal of the American Ceramics Society 69 (1986) C37.

[21] J.D. Fridez, Etude structurale de la déformation superplastique d'une alumine dense à grains fins. Ph. D. thesis, EPFL, Lausanne, Switzerland, 1987.

[22] L.A. Xue, I.W. Chen, Deformation and grain growth of low-temperature-sintered high-purity alumina, Journal of the American Ceramics Society 73 (1990) 3518–3521.

[23] P. Gruffel, Evolutions structurales d'alumine à grains fins dopées à l'yttrium etfluage superplastique. Ph. D. thesis, EPFL, Lausanne, Switzerland, 1991.

[24] F. Wakai, S. Sakaguchi, Y. Matsuno, Suplerplasticity of yttria-stabilized tetragonal ZrO_2 polycrystals [Y-TZP], Adv. Ceram. Mater. 1 (1986) 259–263.

[25] F. Wakai, H. Kato, S. Sagaguchi, Compressive deformation of Y_2O_3-stabilized ZrO_2/Al_2O_3 composite, Yogyo Kyokaishi 94 (1986) 1027–1030.

[26] B.J. Kellett, F.F. Lange, Hot forging characteristics of fine-grained ZrO_2 and Al_2O_3/ZrO_2 ceramics, Journal of the American Ceramics Society 69 (1986) C172.

[27] F. Wakai, T. Iga, T. Nagano, Effect of dispersion of ZrO_2 particles on creep of fine-grained Al_2O_3, Nippon Seramikkusu Kyokai Gakujutsu Ronbunshi 96 (1988) 1206–1209.
[28] F. Wakai, H. Kato, Superplasticity of TZP/Al_2O_3 composite, Adv. Ceram. Mater. 3 (1988) 71–76.
[29] T.G. Nieh, C.M. McNally, J. Wadsworth, Superplastic behaviour of a 20% Al_2O_3/YTZ ceramic composite, Scripta Metallurgica 23 (1989) 457–460.
[30] F. Wakai, Y. Kodama, S. Sakaguchi, N. Murayama, H. Kato, T. Nagano, Superplastic deformation of ZrO_2/Al_2O_3 duplex composites, in: M. Kobayashi, F. Wakai (Eds.) Superplasticity, Materials Research Society, Pittsburgh, PA, 1989, pp.259–266.
[31] J. Wang, R. Raj, Interface effects in superplastic deformation of alumina containing zirconia, titania or hafnia as a second phase, Acta Metall. Mater. 39 (1991) 2909–2919.
[32] D.M. Owen, A.H. Chokshi, The constant stress tensile creep behaviour of a superplastic zirconia–alumina composite, Journal Mater. Sci. 29 (1994) 5467–5474.
[33] J.M. Calderon-Moreno, A.R. Arellano-Lopez, L. Dominguez-Rodriguez, A. Routbort, Microstructure and creep properties of alumina/zirconia ceramics, Journal of the European Ceramics Society 15 (1995) 983–988.
[34] J. Chevalier, C. Olagnon, G. Fantozzi, H. Gros, Creep behaviour of alumina, zirconia and zirconia-toughened alumina, Journal of the European Ceramics Society 17 (1997) 859–864.
[35] J.M. Calderon-Moreno, Influence of ZTA content on the compressive deformation in the Al_2O_3-ZrO_2 (12 mol% CeO2) system, Key Engineering Materials 132–136 (1997) 2088–2091.
[36] O. Flacher, J.J. Blandin, Grain boundary sliding contribution to superplastic deformation in alumina–zirconia composites, Journal Mater. Sci. 32 (1997) 3451–3456.
[37] L. Clarisse, R. Baddi, A. Bataille, J. Crampon, R. Duclos, J. Vicens, Superplastic deformation mechanisms during creep of alumina–zirconia composites, Acta Mater. 45 (1997) 3843–3853.
[38] F. Wakai, A review of superplasticity in ZrO_2-toughened ceramics, Journal Br. Ceram.Trans. 88 (1989) 205–208.
[39] I.W. Chen, L.A. Xue, Development of superplastic structural ceramics, Journal of the American Ceramics Society 73 (1990) 2585–2609.
[40] A.H. Chokshi, Superplasticity in fine grained ceramics and ceramic composites: current understanding and future prospects, Mater. Sci. Eng. A. A166 (1993) 119–133.
[41] A.H. Chokshi, J.R. Porter, Creep deformation of an alumina matrix composite reinforced with silicon carbide whiskers, Journal of the American Ceramics Society 68 (1985) C144.
[42] J.R. Porter, F.F. Lange, A.H. Chokshi, Processing and creep performance of SiC-whisker-reinforced Al_2O_3, Am. Ceram. Soc. Bull. 66 (1987) 343–348.
[43] P. Lipetzky, S.R. Nutt, P.F. Becher, Creep behaviour of an Al_2O_3–SiC composite, Mater. Res. Soc. Symp. Proc. 120 (1988) 271–277.
[44] K. Xia, T.G. Langdon, The mechanical properties at high temperature of SiC-whisker-reinforced Al_2O_3, Mater. Res. Soc. Symp. Proc. 120 (1988) 265–270.
[45] H.T. Lin, P.F. Becher, Creep behaviour of SiC-whisker-reinforced alumina, Journal of the American Ceramics Society 73 (1990) 1378–1381.
[46] A.R. De Arellano-Lopez, F.L. Cumbrera, A. Dominguez-Rodriguez, K.C. Goretta, J.L. Routbort. Compressive creep of SiC-whisker-reinforced Al_2O_3, Journal of the American Ceramics Society 73 (1990) 1297–1300).
[47] H.T. Lin, P.F. Becher, High-temperature creep deformation of alumina–SiC-whisker composites, Journal of the American Ceramics Society 74 (1991) 1886–1893.
[48] P. Lipetzky, S.R. Nutt, D.A. Koester, R.F. Davis, Atmosphere effects on compressive creep of SiC-whisker-reinforced alumina, Journal of the American Ceramics Society 74 (1991) 1240–1247.
[49] A.H. Swan, M.V. Swain, G.L. Dunlop, Compressive creep of SiC whisker-reinforced alumina, Journal of the European Ceramics Society 10 (1992) 317–326.
[50] A.R. De Arellano-Lopez, A. Dominguez-Rodriguez, K.C. Routbort, J.L. Routbort, Plastic deformation mechanisms in SiC-whisker-reinforced alumina, Journal of the American Ceramics Society 76 (1993) 1425–1432.
[51] K. Xia, T.G. Langdon, High temperature deformation of an alumina composite reinforced with silicon carbide whiskers, Acta Metall. Mater. 43 (1995) 1421–1427.
[52] H.T. Lin, K.B. Alexander, P.F. Becher, Grain size effect on creep deformation of alumina–silicon carbide composites, Journal of the American Ceramics Society 79 (1996) 1530–1536.
[53] T. Ohji, A. Nakahira, T. Hirano, K. Niihara, Tensile creep behaviour of alumina/silicon carbide nanocomposite, Journal of the American Ceramics Society 77 (1994) 3259–3262.
[54] Z.Y. Deng, Y.F. Zhang, J.L. Shi, J.K. Guo, Microstructure and flexure creep behaviour of SiC-particle reinforced Al_2O_3 matrix composites, Journal of the European Ceramics Society 16 (1996) 1337–1343.
[55] T. Ohji, T. Hirano, A. Nakahira, K. Niihara, Particle/matrix interface and its role in creep inhibition in alumina/silicon carbide nanocomposites, Journal of the American Ceramics Society 79 (1996) 33–45.
[56] S. Jiao, M.L. Jenkins, W. Davidge, Interfacial fracture energy–mechanical behaviour relationship in Al_2O_3/SiC and Al_2O_3/TiN nanocomposites, Acta Mater. 45 (1997) 149–156.
[57] T. Nagano, H. Kato, F. Wakai, Deformation of alumina/titanium carbide composite at elevated temperatures, Journal of the American Ceramics Society 74 (1991) 2258–2262.
[58] Y. Katsumura, M. Fukuhara, Plastic deformation in Al_2O_3–Ti(C_xN_{1-x}) ceramics, in: P. Vincenzini (Ed.), High Tech. Ceramics, Part C, ed., Elsevier Science, Amsterdam, 1987, pp. 2735–2745.